Journal Pre-proof

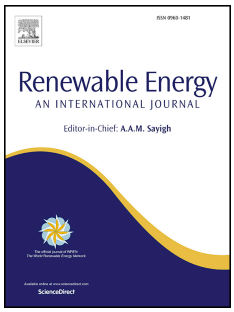

Fragility analyses of offshore wind turbines subjected to aerodynamic and sea wave loadings

Haoran Zuo, Kaiming Bi, Hong Hao, Yu Xin, Jun Li, Chao Li

PII: S0960-1481(20)31142-3

DOI: https://doi.org/10.1016/j.renene.2020.07.066

Reference: RENE 13897

To appear in: *Renewable Energy*

Received Date: 30 May 2019

Revised Date: 11 June 2020

Accepted Date: 13 July 2020

Please cite this article as: Zuo H, Bi K, Hao H, Xin Y, Li J, Li C, Fragility analyses of offshore wind turbines subjected to aerodynamic and sea wave loadings, *Renewable Energy* (2020), doi: https://doi.org/10.1016/j.renene.2020.07.066.

This is a PDF file of an article that has undergone enhancements after acceptance, such as the addition of a cover page and metadata, and formatting for readability, but it is not yet the definitive version of record. This version will undergo additional copyediting, typesetting and review before it is published in its final form, but we are providing this version to give early visibility of the article. Please note that, during the production process, errors may be discovered which could affect the content, and all legal disclaimers that apply to the journal pertain.

© 2020 Published by Elsevier Ltd.

Journal Pre-proof

Haoran Zuo: Conceptualization, Methodology, Software, Validation, Formal analysis, Investigation, Data curation, Writing - original draft. **Kaiming Bi:** Supervision, Writing - review & editing. **Hong Hao:** Supervision, Writing - review & editing. **Yu Xin:** Software. **Jun Li**: Software. **Chao Li**: Methodology.

Journal Pre-proof

Journal Pre-proof

Fragility analyses of offshore wind turbines subjected to aerodynamic and sea wave loadings

Haoran Zuo[a], Kaiming Bi[a,*], Hong Hao[a], Yu Xin[a], Jun Li[a], Chao Li[b]

[a] *Centre for Infrastructure Monitoring and Protection, School of Civil and Mechanical Engineering, Curtin University, Kent Street, Bentley, WA 6102, Australia*

[b] *Faculty of Infrastructure Engineering, Dalian University of Technology, Dalian 116024, China*

[*] *Corresponding author.*

E-mail address: haoran.zuo@curtin.edu.au (H. Zuo), kaiming.bi@curtin.edu.au (K. Bi), hong.hao@curtin.edu.au (H. Hao), yu.xin@postgrad.curtin.edu.au (Y. Xin), junli@curtin.edu.au (J. Li), chao.li@mail.dlut.edu.cn (C. Li).

ABSTRACT

To more effectively extract the vast wind energy in marine areas, offshore wind turbines have been constructed with slender tower and large rotor. External vibration sources such as aerodynamic, sea wave and seismic loadings can threaten the safety of these energy infrastructures. It is important to evaluate the reliability of offshore wind turbines subjected to external vibration sources. Previous research works on the wind turbine fragility analyses only considered the fragility of the tower by assuming the wind turbine was in the parked condition with the blade mass lumped at the top of the tower. The study of the fragility of the blade which is one of the most important components of a wind turbine has not been reported. In the present study, a detailed three-dimensional (3D) finite element (FE) model of the NREL 5 MW wind turbine is developed in ABAQUS, and the tower and blades are explicitly modelled to realistically estimate the aerodynamic loads and structural behaviours of the wind turbine. The uncertainties of the structural mass, stiffness and damping are taken into account to develop the probabilistic wind-induced demand models for the tower and blades. The dynamic behaviours of the wind turbine subjected to the simultaneous aerodynamic and sea wave loadings are investigated in a probabilistic frame and the fragility curves for both the tower and blades under the parked and operating conditions are derived and discussed.

Journal Pre-proof

Keywords: Offshore wind turbine, fragility, tower, blade, aerodynamic load, sea wave load

1. Introduction

Wind energy as one of the renewable energies is becoming a main contributor to the new electricity generation. The growth and expansion of wind farms increased rapidly in the past decade. As reported by the Global Wind Energy Council (GWEC), the worldwide installed capacity of wind power at the end of 2018 reached 591 GW, with an increase of 9.6% compared to that at the end of 2017 [1].

Due to the fact that the power generated by the wind turbine is proportional to the rotor area and cube of wind speed, multi-megawatt wind turbines with slender tower and large rotor are widely constructed in the state-of-the-art designs. These wind turbines are very flexible and lightly damped since they are normally manufactured by the light-weight high-strength materials. They are thus susceptible to external vibration sources such as aerodynamic and sea wave loadings, which are experienced constantly during the whole lifetimes by offshore wind turbines. Moreover, many wind farms are located in the regions of high seismic activities such as western of United States, Japan and China [2], seismic loading is another possible vibration source during their lifetimes in these regions. The excessive vibrations may slow down the conversion of wind energy to electricity, reduce the fatigue life of the structural components or even lead to the structural collapse in extreme conditions.

Extensive research works have been carried out to investigate the dynamic behaviours of wind turbines subjected to aerodynamic, sea wave and/or seismic loadings (e.g. [3-9]). Various control strategies have been proposed to mitigate these adverse vibrations [10-16]. Since the vibration control of wind turbines is beyond the scope of the present study, only the previous studies on the dynamic response analyses of wind turbines are briefly reviewed here. In order to simplify the analysis, the wind turbines were generally assumed in the parked condition, and the blades were modelled as a lumped mass at the top of the tower [12, 14]. In some literatures, the geometrical configurations of the blades were considered and explicitly developed in the finite element (FE) models [17, 18]. However, the influence of the rotation of blades on the structural vibration characteristics was not considered in these studies since they only considered the parked condition. It is well known that the centrifugal stiffness will be generated by the rotating blades and the natural frequencies of the blades therefore

Journal Pre-proof

increase as compared to the parked condition, which in turn affect the dynamic responses of wind turbines [19]. Moreover, the aerodynamic loads acting on the blades are directly related to the geometrical characteristics and rotational velocity of the blades [20]. To more accurately estimate the dynamic behaviours of wind turbines, some researchers modelled the blade as a single or two degrees-of-freedom (DOF) [21, 22] system and investigated the in-plane and/or out-of-plane responses of the blade by using the home-made codes. It should be noted that many mathematics are included in the calculations, and these methods are not convenient for other researchers/engineers to use. Moreover, aerodynamic loads acting along the height of the tower and the length of the blades are unavoidably different, the structural responses thus could not be realistically obtained by using these simplified lumped mass models. Some other researchers (e.g. [23, 24]) modelled the wind turbines by using the open-source program such as FAST. The tower and blades were explicitly developed and the rotation of the blades was considered. However, as explained in the user's guide [25], FAST can only simulate the elastic behaviours of wind turbines. During strong wind events/earthquakes, wind turbines may experience nonlinear deformations, which might not be accurately captured by FAST.

Besides these deterministic analyses, some researchers adopted the probabilistic approach to assess the fragility of wind turbines under aerodynamic, sea wave and/or seismic loadings. For example, Dueñas-Osorio and Basu [26] investigated the unavailability of wind turbines as a function of wind speed. Their investigations indicated that the vibrations of the tower could lead to the malfunction of the acceleration sensitive equipment installed in the nacelle and reduce the annual wind turbine availability. Quilligan et al. [27] used the fragility curves to compare the performances of steel and concrete wind turbine towers subjected to the wind load. Their results showed that the concrete tower performed better than the steel counterpart, however, the extent of improvement was dependent on the type of concrete specified. Mardfekri and Gardoni [28] constructed the probabilistic models for deformation, shear and moment demands on the wind turbine tower to estimate its fragility under wind and sea wave loads, and it was concluded that changing the blade pitch angle could reduce the probability exceeding a predefined limit state of the tower, and sea wave load had a negligible effect on the tower fragility especially under large wind speeds. Kim et al. [29] analysed the seismic fragility of an offshore wind turbine considering the interaction between the monopile foundation and

Journal Pre-proof

surrounding soil, and two different scenarios of applying ground motion were compared. It was found that the seismic response was deeply affected by the way in which ground excitations were applied to the soil spring elements. The influences of near- and far-fault ground motions on the seismic fragility of the wind turbine tower were investigated by Patil et al. [30], and the tower damage was found to be more pronounced in case of near-fault loading events due to the pulse type ground motion. Asareh et al. [31] performed fragility analyses of the tower under the combined wind and earthquake loads, and it was observed that the effect of wind load on the failure probability of the tower was less significant compared to earthquake, which was also confirmed by Yuan et al. [32]. Recently, Hallowell et al. [33] proposed a complete framework for the failure risk quantification of offshore wind turbines subjected to hurricanes. The results of a case study showed that site-specific designs and geometries, intensity measures, fragilities and the ability of the structure to maintain a functional yaw control system influenced the risk of offshore wind turbines to hurricanes.

To mitigate the tower vibrations and further improve the reliability of wind turbine tower, Mensah and Dueñas-Osorio [34] and Fitzgerald et al. [35] installed tuned liquid column dampers (TLCDs) and active tuned mass dampers (ATMDs) in the nacelle, respectively. Moreover, by weighting the wind-induced displacement fragility curves with the likelihood of wind speed realizations at a specific site, the annual failure probabilities of the tower without and with TLCDs were calculated in [34]. Their results underlined that using passive and active controllers could greatly decrease the tower failure risk under the wind load.

However, it should be noted that in the above mentioned studies the wind turbines were either assumed in the parked condition [29] and the mass of the blades was lumped at the top of the tower [28, 30] or the rotation of the blades was considered by the simplified 1- or 2-DOF system [26, 27, 34, 35]. The influence of blades on the structural responses was therefore not necessarily realistically considered as discussed above. Moreover, all these researches focused on the reliability of wind turbine tower, to the best knowledge of the authors, no open literature reports the vulnerability of the blades under the external vibration sources.

In this paper, the dynamic behaviours of the wind turbine subjected to the simultaneous aerodynamic and sea wave loadings are investigated in a probabilistic frame and the fragility curves for both the

Journal Pre-proof

tower and blades under the parked and operating conditions are derived. In particular, the tower and blades of the modern NREL 5 MW wind turbine are explicitly modelled by using the commercially available FE code ABAQUS. The influence of the rotating blades on the aerodynamic loads and dynamic behaviours of the wind turbine is investigated. The uncertainties of the structural mass, stiffness and damping of the wind turbine are considered to derive the probabilistic demand models of the wind turbine as a function of wind speed. The structure of this paper is organized as follows: the properties of the wind turbine, the FE modelling and physical uncertainties are presented in Section 2; Section 3 introduces the external vibration sources, i.e. the aerodynamic and sea wave loadings; the fragility model and numerical results are systematically presented in Section 4 and some concluding remarks are summarized in Section 5.

2. Numerical model description

2.1. NREL 5 MW wind turbine

The NREL 5 MW wind turbine is used as an example in the present study since its detailed information has been well documented and is available to the public. The detailed properties of this wind turbine were reported in [36], and they are tabulated in Table 1. As reported in [36], the pre-twisted blade consists of eight unique airfoil sections, and Fig. 1(a) shows a schematic drawing of the blade. The main geometries of each airfoil section were defined in [36], but the thickness of the blade was not explicitly given. In the present study, a uniform thickness is assumed for the twisted blade, and the mass of each blade is ensured to be the same as that in [36]. This thickness is computed as 0.019 m.

Table 1

Properties of the NREL 5 MW [36]

NREL 5 MW baseline wind turbine properties		
	Rotor diameter	126 m
	Hub height	90 m
	Cut-in, rated and cut-out wind speed	3 m/s, 11.4 m/s, 25 m/s
Blade	Cut-in and rated rotor speed	6.9 rpm, 12.1 rpm
	Length	61.5 m
	Overall (integrated) mass	17,740 kg
	Structural damping ratio	0.5%
	Hub diameter	3 m
Hub and Nacelle	Hub mass	56,780 kg
	Nacelle mass	240,000kg
Tower	Height above water	87.6 m

Journal Pre-proof

	Top outer diameter and wall thickness	3.87 m, 0.019 m
	Bottom outer diameter and wall thicknesses	6 m, 0.027m
	Overall (integrated) mass	347,460 kg
	Structural damping ratio	1%
	Total length	30 m
Monopile	Outer diameter	6 m
	Wall thickness	0.027 m

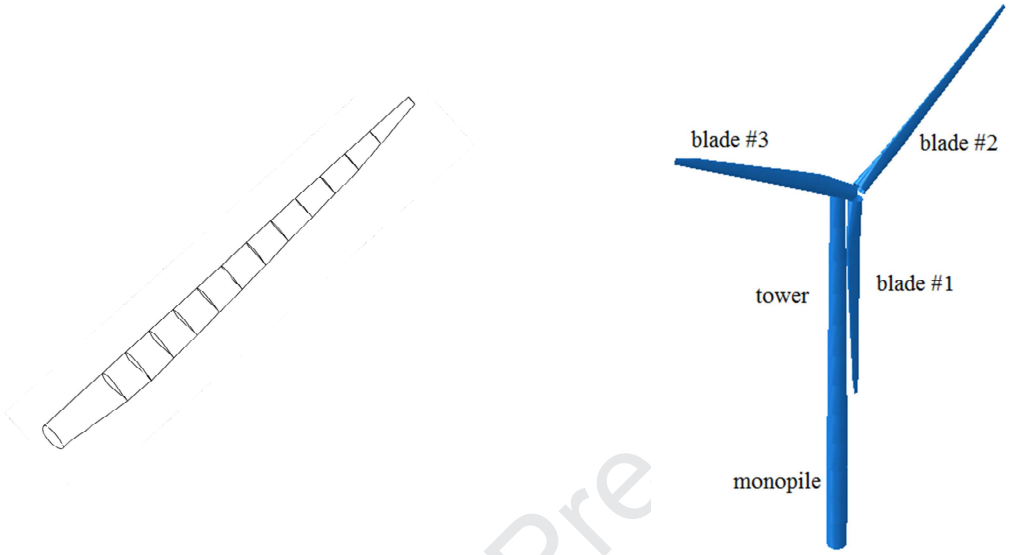

(a) blade (b) FE model

Fig. 1. NREL 5 MW wind turbine: (a) blade and (b) FE model

2.2. FE modelling

The detailed three-dimensional (3D) FE model of the NREL 5 MW wind turbine is developed in ABAQUS. Since the FE model in the present study is exactly the same as that in the authors' previous study [4], the numerical modelling is only briefly introduced herein, interested readers can refer to [4] for more detailed information. The blades, tower and monopile are modelled by shell elements (S4 in ABAQUS). For the hub and nacelle, only the masses of them are considered and they are lumped at the top of the tower. The tower and monopile are connected through a tie constraint, and a hinge connection between the top of the tower and the root of the blades is defined to simulate the operating condition. Fig. 1(b) shows the FE model of the wind turbine, in which the three blades are labelled as #1 to #3 in an anticlockwise direction.

Table 2

Material properties of the wind turbine [36, 37]

Material	Component	Density	Young's	Poisson's	Yield	Plastic

Journal Pre-proof

		(kg/m^3)	modulus (GPa)	ratio	strength (MPa)	strain
Glass/polyester composites	Blade	1850	38	0.3	700	0.02
Steel	Tower	8500	210	0.3	235	0.01
	Monopile	7850	210	0.3	235	0.01

Table 2 tabulates the detailed material properties of the blades, tower and monopile. It should be noted that the vibrating monopile inserted into the seawater can impart an acceleration to the surrounding seawater, and this interaction can be considered by using the added mass model [38]. Therefore, the effective mass of the monopile consists of the physical mass and the added mass, and the latter can be calculated as follows

$$m_a = C_a A_p \rho_w \quad (1)$$

in which, m_a is the added mass, C_a is the coefficient, which is assumed as 1.0 in the present study [39], A_p is the cross-sectional area of the monopile, and ρ_w=1030 kg/m^3 is the density of seawater.

After developing the FE model of the wind turbine, the natural frequencies and mode shapes of the wind turbine were obtained by carrying out an eigenvalue analysis [4]. These results agreed well with those given in [36], which demonstrated the accuracy of the FE model.

2.3. Physical uncertainties

The structural behaviours of the wind turbine are sensitive not only to the variations of the external vibration sources, but also to the inherent uncertainties of the structural properties. In particular, uncertainties in the structural stiffness, masses and damping ratios of the tower and blades can significantly contribute to the variability in the dynamic responses of the wind turbine. In the present study, the variables considered in the simulations include the material (Young's modulus, density, wall thickness) and damping parameters of the tower and blades. The probability density function (PDF) and coefficient of variation (CoV) of the material parameters are tabulated in Table 3. The parameters related to the steel are directly adopted from [27]. For the material of the blades (Glass/polyester composites), the same PDF and CoV are assumed as the steel due to the lack of data.

Table 3

Model input variables

Journal Pre-proof

Material	Variable	Unit	PDF	Mean (μ)	CoV (%)
Steel	Young's modulus	GPa	Lognormal	210	3
	Density	kg/m^3	Normal	8500	1
	Thickness	mm	Normal	30	2
Glass/polyester composites	Young's modulus	GPa	Lognormal	38	3
	Density	kg/m^3	Normal	1850	1
	Thickness	mm	Normal	19	2

The damping mechanism of an offshore wind turbine is composed of structural damping, aerodynamic damping and hydrodynamic damping, which account for the contributions of the structure itself, wind and surrounding sea water respectively. The structural damping ratios of the tower and blades are 1% and 0.5% as reported in [36]. Aerodynamic damping results from the relative velocity between the rotating blades and wind. As suggested by Bisoi and Haldar [40], an aerodynamic damping ratio of 3.5% in the fore-aft direction for an operating wind turbine is adopted. When the wind turbine is in the parked condition, previous studies (e.g. [41]) revealed that the aerodynamic damping is almost zero, and it is adopted in the present study. The hydrodynamic damping results from the drag between the monopile and surrounding sea water and its upper limit is about 0.23% [41]. Summing all the components together, the damping ratio of the tower is 1.23%. For the rotating blades, it is 4% in the fore-aft direction and the value is 0.5% for the parked blades. In the present study, a uniform distribution is assigned to the damping ratios of the tower and blades, and the variability is assumed as 50% with respect to their mean values [26, 35]. The damping of the wind turbine is considered by means of Rayleigh damping and the damping ratio is assumed for the first two vibration modes of the tower and blades.

The Latin Hypercube sampling technique [26] is adopted to obtain the random variables and they are then assigned to the numerical models subjected to different wind speeds within the range from 3 to 25 m/s (within which the wind turbine is allowed to operate).

3. Aerodynamic and sea wave loadings

In the present study, the wind turbine is subjected to the simultaneous aerodynamic and sea wave loadings, which are stochastically simulated according to the sophisticated simulation techniques. The detailed simulation techniques have been introduced in the authors' another paper [4]. For

Journal Pre-proof

completeness of the present paper, they are briefly introduced in this section. Interested readers can refer to [4] for more detailed information.

For the aerodynamic load acting on the tower, it can be decomposed into a mean and a fluctuating component. The fluctuating aerodynamic loads at different locations along the tower are different but with certain similarities, which is known as the spatial correlation effect. It can be described by a spatial coherency loss function. The power spectral density (PSD) of the fluctuating wind speed at any locations can be calculated by using the Kaimal spectrum [19],

$$S_{vv}(h,f) = \frac{v_*^2}{f}\frac{200c}{(1+50c)^{5/3}} \tag{2}$$

in which, v_* is the friction velocity, f is the frequency in Hz, and c is the Monin coordinate, which is given by Eq. (3)

$$c = fh/\bar{v}(h) \tag{3}$$

where h is the height of the location where aerodynamic load is calculated, $\bar{v}$ is the mean wind speed and it can be calculated by Eq. (4)

$$\bar{v}(h) = v_* \ln(h/z_0)/K \tag{4}$$

where K is the von-Karman's constant and z_0 is the roughness length.

The tower is generally divided into several segments to simplify the simulation of the aerodynamic load on the tower. Ideally the finer the segment, the more accurate the aerodynamic load would be estimated. To investigate the influence of segment number on the aerodynamic load simulation, a numerical convergence test is performed. The results show that the variations of the aerodynamic load on the tower decrease with the increasing of segment number, and the total load is consolidated when the tower is divided into nine segments. To balance the computational time and accuracy, nine segments with a length of 10 m are adopted in the present study to simulate the aerodynamic load on the tower. On the other hand, it should be noted that the adopted number of segments in the present study may not be applied to other wind turbines especially the height of the wind turbine tower is significantly different from the current one, which should be determined case by case.

Fig. 2 shows the fluctuating wind speed PSDs in the top segment (85-90 m along the tower) and the corresponding model values, which are calculated by Eq. (2), when the mean wind speeds at the hub

height are 3 and 25 m/s respectively. As shown, the simulated results are in well agreement with the corresponding model values. For conciseness, not all the aerodynamic loads on the tower are shown, only the time histories in the top segment are shown in Fig. 3 when the mean wind speeds at the hub height are 3 and 25 m/s respectively.

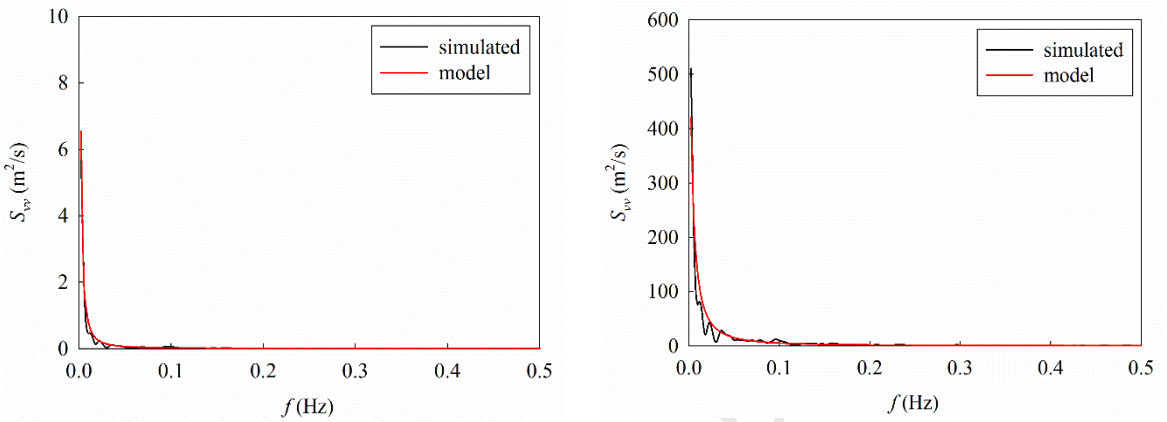

(a) v=3 m/s (b) v=25 m/s

Fig. 2. Comparisons between the simulated and model PSDs of wind speed

Different from the aerodynamic load on the tower, the aerodynamic loads on the blades are influenced by the wind speed, rotational velocity, pitch angle and geometrical characteristics of the blade. Blade Element Momentum (BEM) method [20] is adopted in the present study to estimate the aerodynamic loads on the blades. In this method, it is assumed that no aerodynamic interaction between different sections along the rotor, the blade therefore can be divided into several elements and the aerodynamic load acting on each element can be calculated separately.

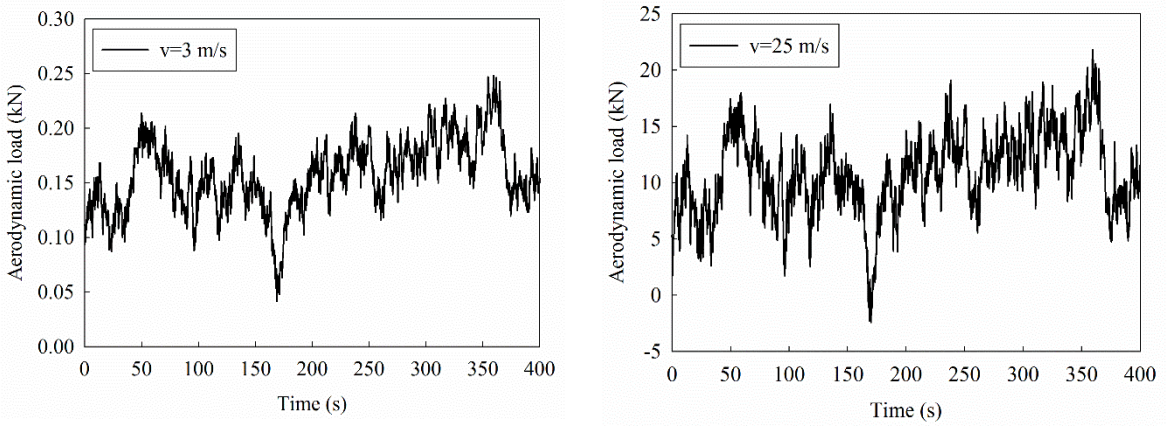

(a) v=3 m/s (b) v=25 m/s

Fig. 3. Aerodynamic load time histories at the top of the tower

The relative wind velocity on each element of the blade (v_{rel}) is given by

$$v_{rel}(r) = \sqrt{\left(\bar{v}(1-a) + v_f\right)^2 + \left(\Omega r(1+a')\right)^2} \tag{5}$$

where r is a radial distance of the element from the centre of the hub, a and a' are the axial and tangential induction factors respectively, Ω is the rotational velocity in rad/s and v_f is the fluctuating wind speed. It should be noted that the PSD of the fluctuating wind speed is a time-variant spectrum due to the height of the blade experiences a sinusoidal variation in magnitude with the rotation of the blades. Not to further complicate the problem, an isotropic, homogenous wind turbulence at the height of the hub is assumed to represent the wind turbulence over the rotor field in the present study. According to this assumption, the fluctuating wind speed in Eq. (5) can be easily calculated by using the PSD of wind velocity at the hub height defined in Eq. (2).

After the relative wind speed is determined, the local lift and drag forces on each element then can be computed as follows

$$p_l(r) = \frac{1}{2}\rho v_{rel}^2(r) l(r) C_{lb} \tag{6}$$

$$p_d(r) = \frac{1}{2}\rho v_{rel}^2(r) l(r) C_{db} \tag{7}$$

In Eqs. (6) and (7), ρ is the air density, l is the chord length and C_{lb} and C_{db} are the lift and drag coefficients of the blade respectively, which are related to the flow, pitch and pre-twist angles. Fig. 4 shows the flap-wise and edgewise aerodynamic loads on the blade #2 when the mean wind speeds at the hub height are 3 and 25 m/s respectively.

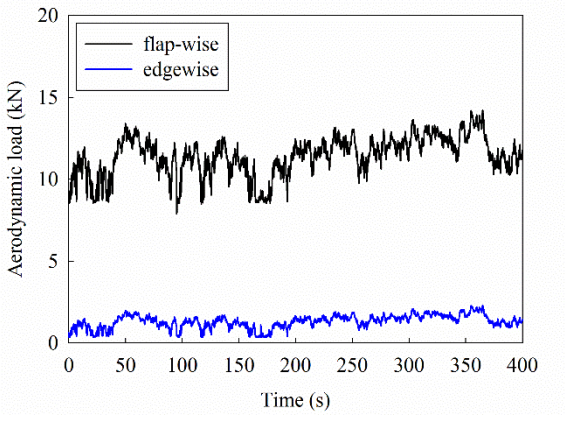

(a) v=3 m/s

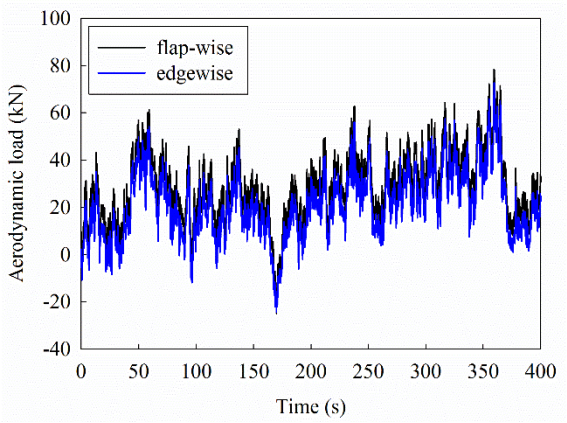

(b) v=25 m/s

Journal Pre-proof

Fig. 4. Flap-wise and edgewise aerodynamic loads on the blade #2

For the sea wave loading acting on the monopile, the JONSWAP spectrum [42] is used to simulate the sea surface elevation and it can be described by Eq. (8)

$$S_{\eta\eta}(f) = \alpha_P g^2 (2\pi)^{-4} f^{-5} exp\left[-\frac{5}{4}\left(\frac{f_m}{f}\right)^4\right] \gamma^{exp\left[-\frac{(f-f_m)^2}{2\sigma^2 f_m^2}\right]} \quad (8)$$

in which g is the gravitational acceleration and γ is the peak enhancement factor and a value of 3.3 is used in the simulation. α_P, f_m and σ are three constants, which are

$$\alpha_P = 0.076(Fg/v_{10}^2)^{-0.22} \quad (9)$$

$$f_m = 11(v_{10}F/g^2)^{-1/3}/\pi \quad (10)$$

$$\sigma = \begin{cases} 0.07 & f \le f_m \\ 0.09 & f > f_m \end{cases} \quad (11)$$

In Eqs. (9-11), F is the fetch length and v_{10} is the mean wind speed at 10 m above the sea surface, which can be determined by Eq. (4).

The sea wave length is much larger than the dimension of the monopile [4], Morison equation (Eq. (12)) therefore can be adopted to calculate the sea wave load on the monopile

$$F_w = \frac{1}{2}\rho_w C_{dp} d_p |v_x| v_x + \rho_w C_m A_p a_x \quad (12)$$

where F_w is the transverse sea wave load per unit length of the monopile, ρ_w is the seawater density, d_p and A_p are the outer diameter and cross-sectional area of the monopile respectively, v_x and a_x are the velocity and acceleration of water particles respectively, and the detailed calculation of these two parameters can be found in [4] and is not introduced herein. C_{dp} and C_m are the drag and inertia coefficients respectively, and they are as functions of Reynolds number, the Keulegan-Carpenter number and the roughness [39]. The uncertainties of these two parameters may also influence the fragility curve, which are however not considered in the numerical simulations, and fixed values of 1.2 and 2.0 as suggested in [39] are adopted in the present study.

Similar to the tower, the monopile in the seawater is equally divided into two segments. Fig. 5 shows the simulated sea wave load time histories at the mean sea level when the mean wind speeds at the hub height are 3 and 25 m/s respectively and Fig. 6 compares the PSDs of the simulated sea surface elevation and the model. Good matches are observed as shown.

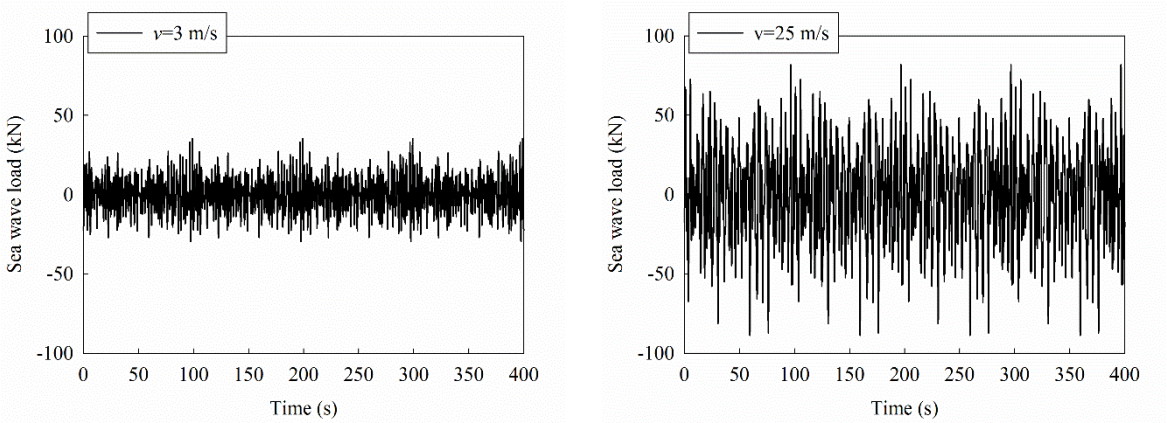

(a) v=3 m/s (b) v=25 m/s

267 Fig. 5. Sea wave load time histories at the mean sea level

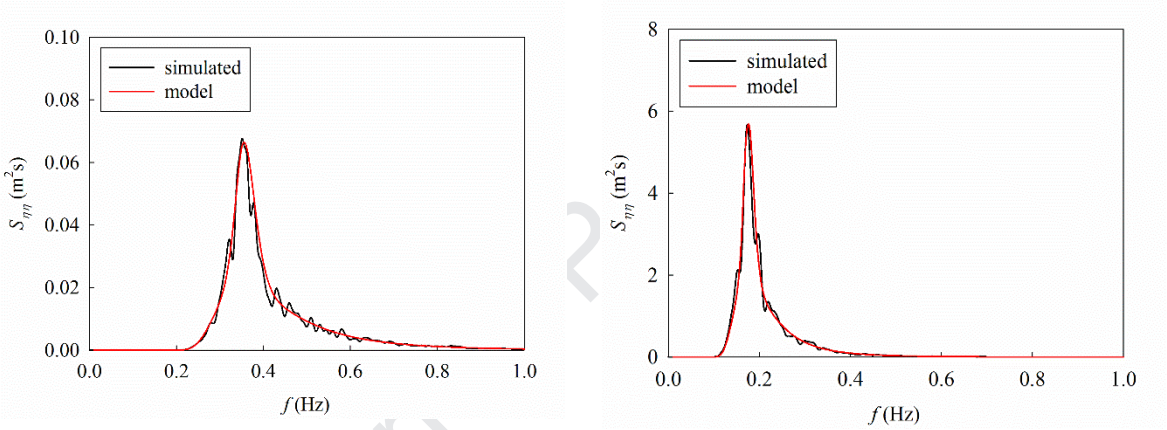

(a) v=3 m/s (b) v=25 m/s

268 Fig. 6. Comparisons between the simulated and model PSDs of sea surface elevation

269 As introduced above, the tower, blade and monopile are divided into several segments in the
270 simulation of the aerodynamic and sea wave loadings. In the FE model, a reference point is developed
271 in each segment and coupled to the cross section of the corresponding segment, the simulated
272 aerodynamic and sea wave loadings are applied to these reference points as the external loadings.

273 **4. Fragility analysis of wind turbine**

274 ***4.1. Fragility function***

275 The structural fragility can be defined as the conditional probability of a structural demand to reach or
276 exceed the structural capacity at a given excitation level. The present study constructs the fragility
277 curves of the tower and blades by using the out-of-plane displacement responses obtained from the
278 numerical simulations. For the fragility curve calculated based on the in-plane responses of the blades,

Journal Pre-proof

they are not included in the present study due to the lack of data to define the corresponding limit state levels.

In seismic response analysis, fragility curves can normally be generated by using the incremental dynamic analysis (IDA) method or the probability seismic demand analysis (PSDA) method [43]. In the former approach, all motions are scaled to the selected intensity levels and IDA is performed at different hazard levels. A large amount of numerical simulations are needed in order to generate the fragility curve by using the IDA method. On the other hand, the PSDA approach uses unscaled earthquake ground motions and regression analysis to obtain the mean and standard deviation of the structural response at each intensity level by assuming a logarithmic correlation between the median engineering demand parameters and a selected intensity level. Compared to the IDA approach, the PSDA method requires much less computational effort, but can result in reasonable estimations of the fragility curve [43]. It is therefore widely used in the fragility analyses for engineering structures when they are subjected to the earthquake loadings. Recently, the PSDA method is also adopted in the wind-induced fragility analyses of wind turbines [26, 34, 35]. In the present study, the PSDA method is used and the mean wind speed at the hub height is selected as the fragility hazard parameter though the aerodynamic and sea wave loadings are considered in the analyses due to the fact that the structural responses induced by the sea wave load are much smaller than those induced by the aerodynamic load [4]. Similar to the seismic demand model developed in [44, 45], the structural demands for a wind turbine under the combined wind and sea wave excitations are estimated by using a power law functional form as

$$D_w = m(v_w)^n \; or \; ln(D_w) = lnm + nln(v_w) \tag{13}$$

where D_w is the median wind-induced out-of-plane displacement of the wind turbine, v_w is the mean wind speed at the hub height, and m and n are coefficients obtained from regression analysis.

The power law model (Eq. (13)) is used to develop the fragility curves by providing an estimation of the likelihood of displacement threshold exceedance as a function of wind speed. The conditional probability of exceeding a prescribed displacement is defined as a lognormal distribution:

Journal Pre-proof

$$P[D_w > D_{LS}|v_w] = \Phi\left(\frac{ln(D_w) - ln(D_{LS})}{\beta_{D_w|v_w}}\right) \quad (14)$$

In Eq. (14), D_{LS} represents the displacement threshold that initiates changes in the performance state of the wind turbine, $\Phi(\cdot)$ is the standard normal cumulative distribution function, $\beta_{D_w|v_w}$ is the dispersion of the logarithmic displacement response as a function of wind speed. For simplicity, it is normally assumed that the parameter $\beta_{D_w|v_w}$ is independent of v_w and can be expressed by Eq. (15) [45]

$$\beta_{D_w|v_w} = \sqrt{\frac{\sum_{j=1}^{N}\left[ln(D_j) - ln(D_{wj})\right]^2}{N-2}} \quad (15)$$

where D_j is the jth realization of the wind-induced structural demand, D_{wj} is the median displacement of the wind turbine corresponding to the jth wind speed and can be calculated by Eq. (13), and N is the number of conducted nonlinear time history analyses. In the present study, 45 nominally identical but statistically different wind turbine models are generated based on the random variables defined in Section 2.3, and these 45 wind turbine models are paired with 45 different wind speeds to calculate the structural responses and further estimate the fragility curves.

4.2. Limit state levels

To assess the safety of the wind turbine subjected to the aerodynamic and sea wave loadings, limit states should be defined. Four limit states are widely adopted in the analyses of offshore wind turbines, which are the serviceability limit state (SLS), ultimate limit state (ULS), fatigue limit state (FLS) and accidental limit state (ALS) [46]. The SLS and ULS are considered in the present study to determine the damage levels of the wind turbine. The SLS is the deformation tolerances to ensure the regular and normal operation of the wind turbine and the ULS corresponds to the maximum load-carrying capacity (e.g. yielding, buckling, overturning etc.) of a structure and structural components. In the present study, a damage criterion based on the displacements at the top of the tower and the tip of the blade is adopted and four damage states are defined depending on the different demand parameters of the wind turbine. These four damage states are introduced individually as follows:

Damage state one (DS_1) corresponds to the SLS. The deformation tolerance is usually defined in the design basis and it is often specified in terms of the maximum allowable rotation of the pile head at

Journal Pre-proof

the seabed in a vertical plane. DNV [46] specifies that the maximum allowable tilt of the tower should be less than 0.5°, which incorporates the error during the construction and it normally ranges from 0.2° to 0.25°. The maximum allowable tilt of the tower due to external vibration sources is therefore about 0.25°. In the present study, the height of the wind turbine is near 120 m, so the tilt of the tower can be converted to the displacement at the top of the tower, and it is 0.524 m.

To determine the other three damage states of the tower, pushover analysis is carried out to investigate the nonlinear deformation characteristics of the wind turbine tower and to find the corresponding critical displacement. This procedure is achieved by gradually increasing the displacement applied in the for-aft direction at the top of the tower and considering the first buckling mode as initial imperfection [47]. It is obvious that the maximum internal forces (bending moment and shear force) appear at the bottom of the monopile. The results from the pushover analysis can describe the relationship between the internal forces at the bottom of the monopile and the displacement at the top of the tower. The normal stress is adopted as the yield criterion for the wind turbine in the present study, which can be calculated by

$$\sigma = \frac{M}{W} - \frac{N}{A} \tag{16}$$

$$W = \frac{\pi d_1^3}{32}\left[1 - \left(\frac{d_2}{d_1}\right)^4\right] \tag{17}$$

$$A = \frac{\pi}{4}(d_1^2 - d_2^2) \tag{18}$$

in which M is the bending moment as shown in Fig. 7(a), N is the axial force, d_1 and d_2 are the outer and internal diameters of the monopile respectively.

Fig. 7(a) shows the relationship between the bending moment/shear force at the bottom of the monopile and the displacement applied at the top of the tower. By substituting them into Eqs. (16-18), the normal stress at the bottom of the monopile can be obtained and it is presented in Fig. 7(b). As shown, nonlinear behaviour begins to occur at a displacement of 2.097 m, which indicates that the wind turbine tower starts to yield at this displacement. It also can be observed that the internal force/stress-displacement relationship shows a snap-back behaviour due to the local buckling of the tower when the displacement at the top of the tower reaches 2.922 m. Fig. 8 shows the local buckling

of the wind turbine from the pushover analysis, in which the blades are not presented to more clearly show the result. As shown, the buckling of the wind turbine appears at a point approximately 10 m above the bottom of the monopile foundation, which is consistent with previous studies (e.g. [31]).

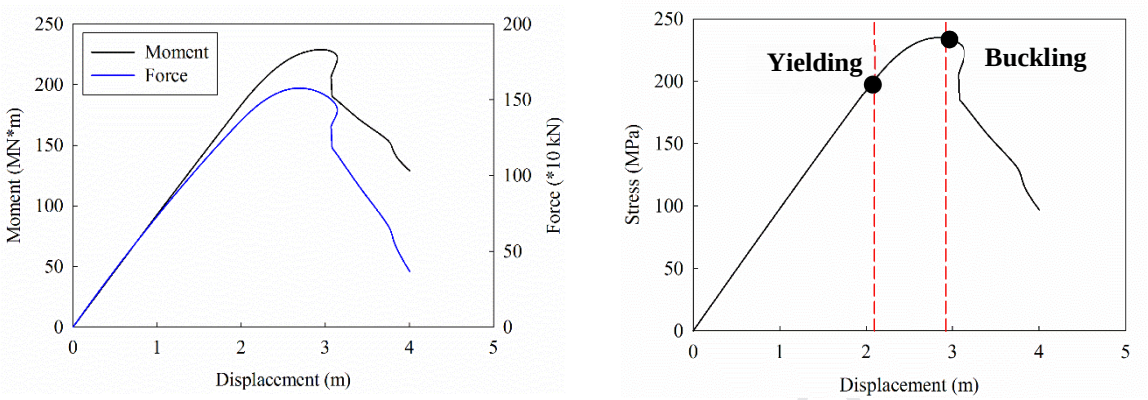

(a) bending moment and shear force (b) stress

Fig. 7. Moment, shear force and stress and displacement relationship from pushover analysis

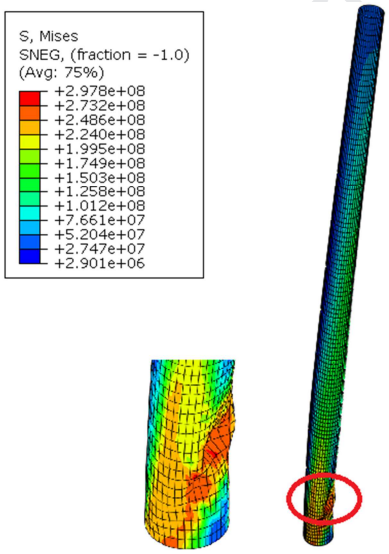

Fig. 8. Buckling of the wind turbine tower (deformation is amplified three times)

The above results show that buckling occurs at a much larger displacement compared to the yielding. In the present study, wind and wave loadings are considered as excitations, buckling is very unlikely to appear, and it is not adopted as a damage state. Following the suggestions of many researchers (e.g. [29, 34]), damage states DS_2-DS_4 are defined as 30%, 40% and 50% of the yielding displacement of the tower, which are 0.629 m, 0.839 m and 1.049 m respectively. Table 4 tabulates the four limit states of the wind turbine tower. However, it is worth noting that when the wind turbine has opening

Journal Pre-proof

and stiffening [47, 48] or it is subjected to other vibration sources such as earthquake, buckling might occur, and it should be considered as a limit state in the analyses.

Table 4

Damage states of the wind turbine tower

Damage states	Critical displacement	Description
DS_1	0.524 m	SLS
DS_2	0.629 m	30% of yield stress
DS_3	0.839 m	40% of yield stress
DS_4	1.049 m	50% of yield stress

Different from the tower, it is not realistic to define the damage limit states (the critical displacement) of the blade by using the pushover method, since the blade is made of high-strength material (e.g. for the glass/polyester composites, the yield strength is 700 MPa [37]), which is very difficult to yield. On the other hand, a minimum clearance between the tip of the blade and the tower should be specified to avoid the possible collision between the rotor and the tower during the extreme conditions. A tilt angle of 5° between the rotor axis and the horizontal plane is used in the design of the wind turbine [49]. As shown in Table 1, the rotor radius is 63 m, so the maximum allowable displacement at the tip of the blade subjected to the external loads is 5.5 m. Similar to the limit states of the tower as defined above, the four limit states for the blade are defined as 20%, 30%, 40% and 50% of the maximum allowable displacement at the tip of the blade (i.e. 5.5 m), which are 1.100, 1.650, 2.200 and 2.750 m respectively.

4.3. Fragility curves of the wind turbine

Based on the prescribed damage states of the tower and blades, the fragility curves of the wind turbine can be calculated by using Eqs. (13) and (14). To examine the influence of operational conditions on the fragility curves of the wind turbine, two scenarios are considered. In the first scenario, the wind turbine is in the parked condition with the locations of the blades shown in Fig. 1(b). In the second scenario, the blades are rotating at a uniform velocity, which is related to the wind speed. For the NREL 5 MW wind turbine, the blades start to rotate at a cut-in velocity of 6.9 rounds per minute (0.72 rad/s) when the wind speed is 3 m/s, and the maximum wind energy output will be achieved at a rated velocity of 12.1 rounds per minute (1.27 rad/s) when the wind speed is or above 11.4 m/s. The

Journal Pre-proof

rotational velocity is assumed as a linear variation between the cut-in and rated velocities. In the present study, the wind speeds ranging from 3 to 25 m/s with an interval of 0.5 m/s are considered (in total 45 wind speeds, i.e. N=45 in Eq.(15)), which correspond to the normal operating range of the wind turbine. The aerodynamic and sea wave loads shown in Figs. 3 and 5 are applied to the tower. For the aerodynamic loads on the blades, they depend on the rotational velocity as introduced in Section 3. Different aerodynamic loads on the blades are simulated according to the different wind speeds and rotational velocities. It should be noted that the fragility of the wind turbine is related to the maximum structural response, which is influenced by the duration of the external excitations. All the numerical results in the present study are based on a relatively long duration of 400 s as shown in Section 3.

4.3.1. Parked condition

It is obvious that the maximum responses of the tower and blades occur at the top of the tower and the tip of the blade when the wind turbine is subjected to the simultaneous aerodynamic and sea wave loadings. Here only the maximum responses of the tower and blades are used to develop the fragility curves. Fig. 9 shows the peak displacements at the top of the tower under different wind speeds and the probabilistic wind-induced demand model (red curve) constructed based on the regression analysis (Eq. (13)) by using these maximum displacements. The values of the parameters m, n and $\beta_{D_w|v_w}$ are tabulated in Table 5. As shown in Fig. 9, the power law model can well describe the relationship between the displacement response at the top of the tower and the wind speed with a coefficient of determination R^2 equalling to 0.9879. It also can be seen that the uncertainties in the Young's modulus, wall thickness, density and damping ratio of the tower marginally affect the displacement responses of the tower when the wind speed is below 10.5 m/s. This is because the displacements at the top of the tower are small when the wind speeds are low. With the increment of the wind speed, the uncertainties of these parameters have more obvious effect on the responses of the tower and the dispersion of the displacement responses becomes larger.

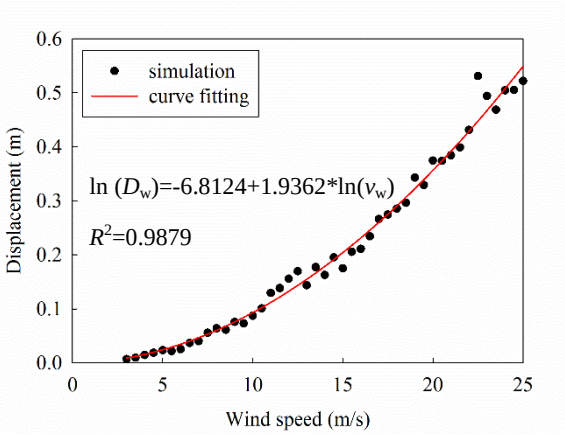

Fig. 9. The maximum displacements at the tower top and the corresponding wind-induced demand model in the parked condition

Table 5

Parameters to characterize wind-induced displacement fragility curves in the parked condition

Component	m	n	$\beta_{D_w \mid v_w}$
Tower	0.0011	1.9362	0.1252
Blade #1	0.0017	2.1319	0.2479
Blade #2 (#3)	0.0021	2.1001	0.2115

Fig. 10 shows the maximum displacements at the tips of the blades under different wind speeds and the corresponding probabilistic wind-induced demand models. The values of the parameters for the demand models are also tabulated in Table 5. It should be noted that the displacement responses of blade #3 are the same as those of blade #2 due to the fact that the geometrical configurations and locations of blades #2 and #3 are symmetric as shown in Fig. 1, and the same excitations are applied on those two blades. As shown in Fig. 10, the coefficients of determination R^2 in the probabilistic wind-induced demand models of blades #1 and #2 are 0.9466 and 0.9415 respectively, which again indicate the good fits of the model to the simulated responses of the blades. It also can be observed from Fig. 10 that the maximum displacements at the tip of blade #1 are slightly smaller than those at the tip of blade #2 since blade #1 locates at a lower position than blade #2 and the aerodynamic loads acting on blade #1 are smaller than those on blade #2 for a particular wind speed. Comparing Fig. 10 with Fig. 9, it can be seen that the dispersion of the displacement responses of the blades is larger than that of the tower. This is because as tabulated in Table 3, although the PDF and CoV of the blade parameters are assumed the same as those of the tower, the mean value of the Young's modulus of the

blade is 38 GPa, which is much smaller than that of the tower of 210 GPa. A small variation on the input values will result in more obvious structural response changes, which in turn leads to the larger dispersion of the displacement responses of the blades as compared to the tower.

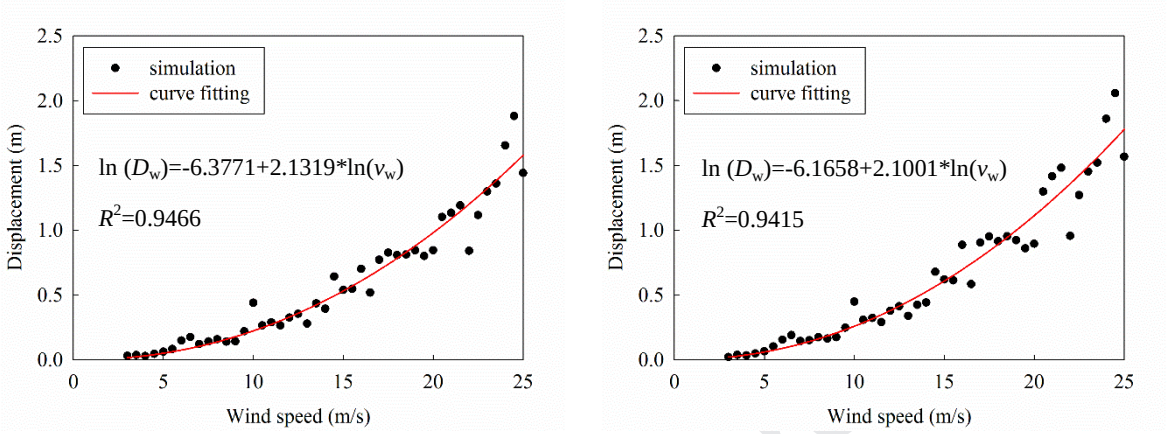

(a) blade #1 (b) blade #2 (#3)

Fig. 10. The maximum displacements at the blade tips and the corresponding wind-induced demand models in the parked condition

After the probabilistic wind-induced demand models of the tower and blades are determined, the fragility curves of the tower and blades with respect to different damage states can be calculated by using Eq. (14). Figs. 11 and 12 show the fragility curves of the tower and blades respectively when the wind turbine is in the parked condition. For brevity, only the fragilities of the wind turbine at the cut-in (3 m/s), rated (11.4 m/s) and cut-out (25 m/s) wind speeds are discussed below.

As shown in Figs. 11 and 12, the likelihood of exceeding the four prescribed displacement levels is near zero for the tower and blades at the cut-in and rated wind speeds of the parked wind turbine. When the wind speed is 25 m/s, Fig. 11 shows that the damage probabilities of the tower are 70.2%, 17.6%, 0.1% and 0%, respectively for the four displacement thresholds, which indicates that the tower is very unlikely to yield under this wind condition. It might be worth reiterating that buckling occurs at a much larger displacement (2.922 m as shown in Fig. 8) than that when yielding occurs (2.097 m), thus the wind turbine tower is also less likely to fail as a buckling damage, which supports the selection of limit states as presented in Section 4.2. For the blades, Fig. 12 shows that the probabilities of the limit state exceedance for blade #1 are 94.2%, 47.5%, 11.1% and 1.7% respectively and they are 99.1%, 67.1%, 17.9% and 2.4% respectively for blade #2 when the wind speed reaches 25 m/s.

The probabilities of exceeding the predefined displacement thresholds of blade #2 are higher than those of blade #1 since the displacement responses of blade #2 are larger as discussed above. The results also show that the potentials of the blade crossing the four limit states are all higher than the tower. This is actually deemed necessary and reasonable, since the blades are supported by the tower, the damage of the tower will lead to the total malfunction of the wind turbine. The tower therefore can be regarded as a more important component than the blades, and it should be designed with higher reliability.

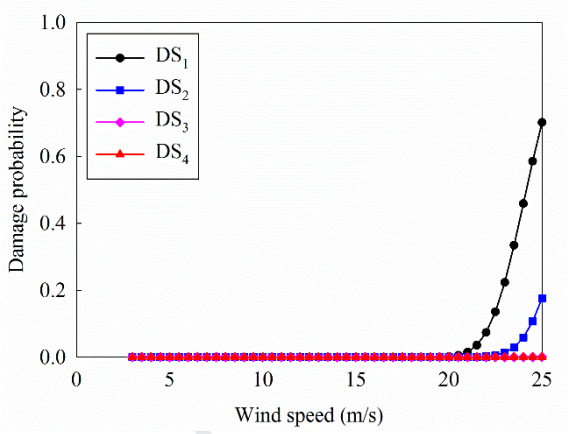

Fig. 11. Wind-induced fragility curves for the tower in the parked condition.

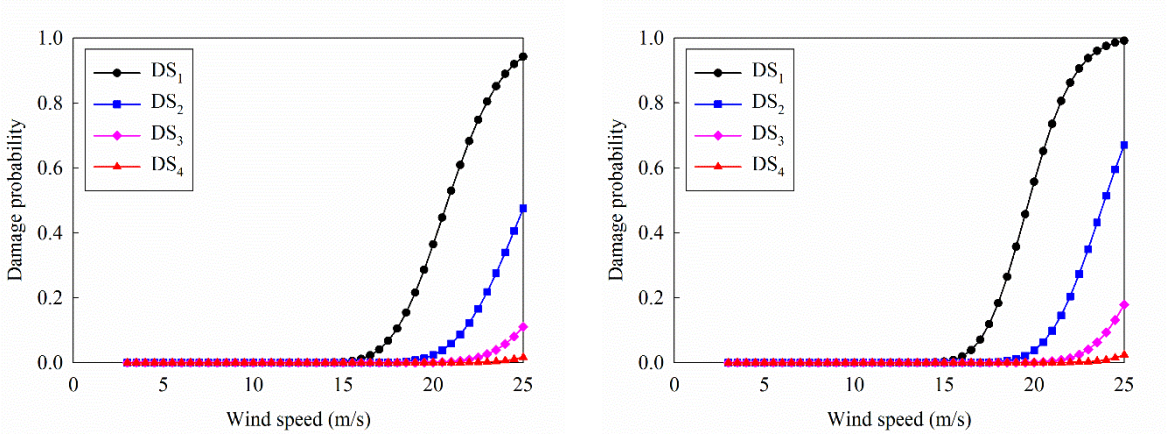

(a) blade #1 (b) blade #2 (#3)

Fig. 12. Wind-induced fragility curves for the blades in the parked condition

4.3.2. Operating condition

This section presents the fragility of the operating wind turbine under the simultaneous aerodynamic and sea wave loadings. Fig. 13 shows the peak displacements at the top of the tower under different wind speeds and the fitted probabilistic wind-induced demand models. Table 6 tabulates the values of

the parameters m, n and $\beta_{D_w|v_w}$ from regression analyses. It can be seen that the dispersion of the maximum displacements at the top of the tower in the operating condition is larger than that of the parked wind turbine as shown in Fig. 9. This is because the aerodynamic loads on the rotating blades are larger than those on the parked blades, which results in more severe interaction between the top of the tower and the root of the blades.

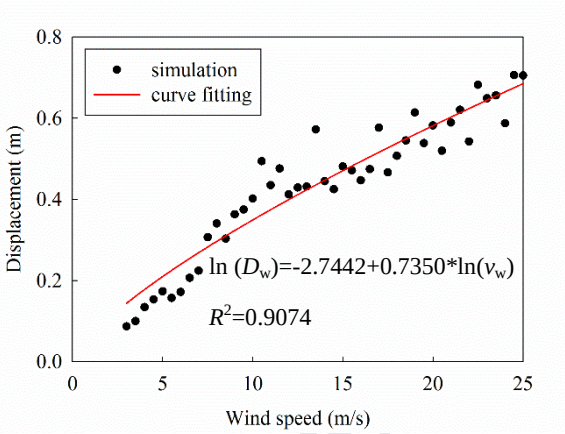

Fig. 13. The maximum displacements at the tower top and the corresponding wind-induced demand model in the operating condition

Table 6

Parameters to characterize wind-induced displacement fragility curves in the operating condition

Component	m	n	$\beta_{D_w|v_w}$
Tower	0.0643	0.7350	0.1810
Blade #1	0.4420	0.4593	0.2075
Blade #2	0.5438	0.3989	0.1809
Blade #3	0.5816	0.3730	0.1874

Fig. 14 shows the maximum displacements at the tips of the blades under different wind speeds and the corresponding probabilistic wind-induced demand models. The fitted values are also tabulated in Table 6. As shown in Fig. 14 and Table 6, different from the displacement responses of the blades in the parked condition, when the blades are rotating, the displacements at the blade tips increases at a slow rate with the increasing of the wind speed, i.e. n<1 as tabulated in Table 6. This is because the aerodynamic damping in the parked condition is about zero, however, as stated in Section 2.3, the aerodynamic damping appears due to the rotation of the blades, and this damping is related to the rotational velocity and wind speed. Large rotational velocity and wind speed result in large

aerodynamic damping, which slows down the increasing rate of the displacement responses of the blades. Moreover, the pitch control mechanism in the blades is initiated when the wind speed is above the rated speed to limit the aerodynamic loads acting on the blades and maintain wind energy output by changing pitch angles during operation, which is considered in the simulation of the aerodynamic loads in the present study. As shown in Fig. 14, the maximum displacement responses of the three blades are slightly different when the wind turbine is in the operating condition. This is because of the influence of the initial positions of the blades.

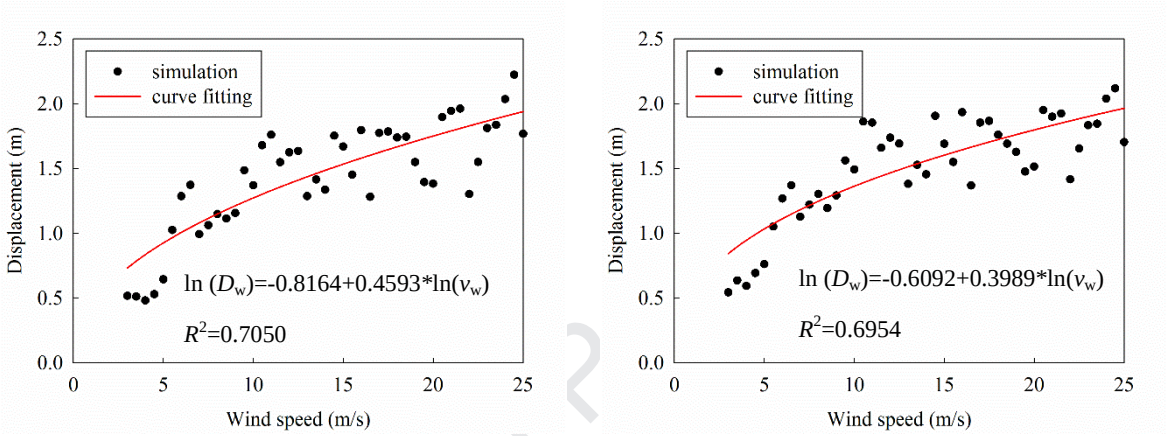

(a) blade #1 (b) blade #2

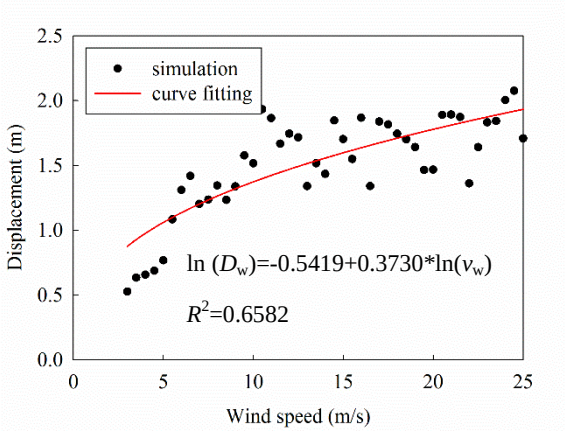

(c) blade #3

Fig. 14. The maximum displacements at the blade tips and the corresponding wind-induced demand models in the operating condition

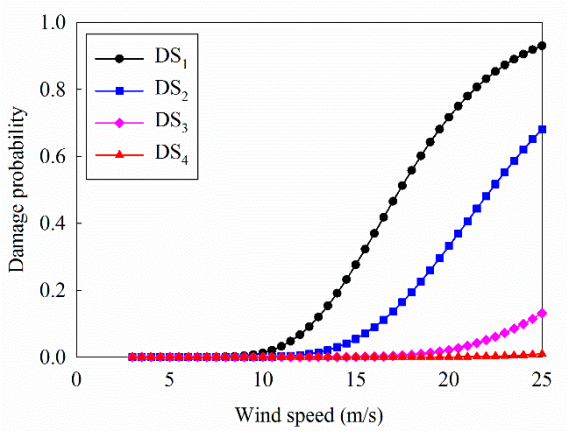

Fig. 15. Wind-induced fragility curves for the tower in the operating condition

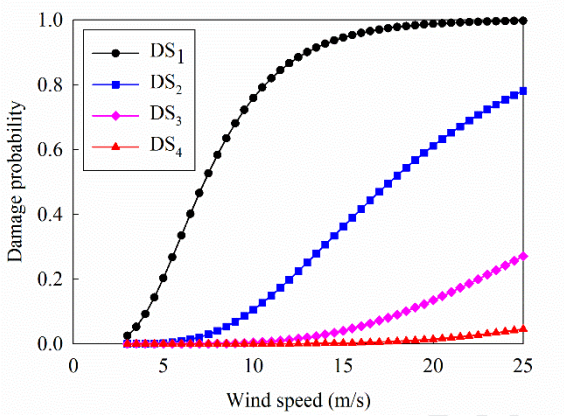

(a) blade #1

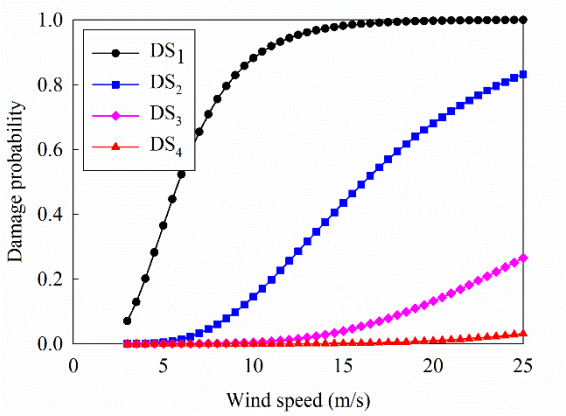

(b) blade #2

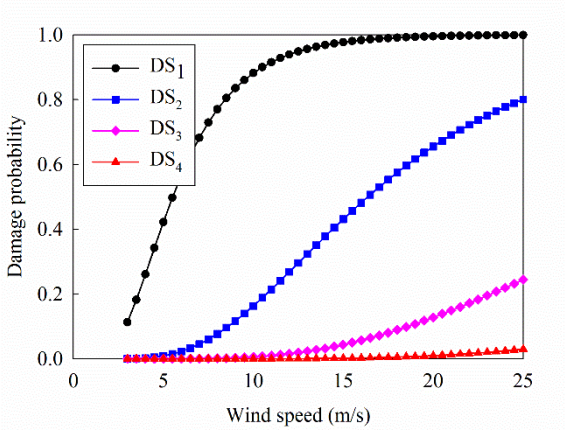

(c) blade #3

Fig. 16. Wind-induced fragility curves for the blades in the operating condition

Figs. 15 and 16 show the fragility curves of the tower and blades respectively when the wind turbine is in the operating condition. As shown in Fig. 15, the likelihood of exceeding the prescribed limit states of the tower is about zero when the wind speed is 3 m/s. When the wind turbine is subjected to

Journal Pre-proof

the rated speed of 11.4 m/s, the damage probabilities of the tower are 4.7%, 0.4%, 0% and 0% respectively. When the wind speed increases to 25 m/s, they become 93.1%, 68.1%, 13.1% and 0.9% respectively. Compared to the parked condition, it can be seen that the probabilities of exceeding DS_1-DS_4 are larger in the operating condition, this is because larger aerodynamic loads acting on the wind turbine lead to larger median displacement responses of the tower as shown in Fig. 13.

As shown in Fig. 16, when the wind speed is 3 m/s, the probability of reaching DS_1 for the three blades are 2.5%, 7.1% and 11.2% respectively and the likelihood of exceeding the other three states is near zero. When the wind turbine is operating under the rated speed of 11.4 m/s, the damage probabilities of blade #1 are 84.4%, 17.3%, 1.0% and 0% respectively for the four displacement thresholds defined above. For the blade #2, they are 93.2%, 22.7%, 1.0% and 0% respectively and the corresponding values are 92.8%, 24.1%, 1.3% and 0% for blades #3. When the wind speed is 25 m/s, the damage probabilities of blade #1 are 99.7%, 78.1%, 27.1% and 4.6% respectively. For blade #2, the corresponding values are 99.9%, 83.2%, 26.5% and 3.1% and they are 99.9%, 80.0%, 24.4% and 3.0% respectively for blade #3. Similar to the tower, the probabilities of DS_1-DS_4 exceedance of the rotating blades are larger than those of the parked blades, which can be explained again by the larger median displacement responses (refer to Figs. 10 and 14).

5. Conclusions

In this paper, the dynamic behaviours of the NREL 5 MW wind turbine subjected to the simultaneous aerodynamic and sea wave loadings are investigated by taking the uncertainties of the material and damping into account. Different damage states for the tower and blades are defined based on the serviceability and ultimate limit states. The fragility curves of the tower and blades are developed. Numerical results show that:

(1) The uncertainties of the material and damping ratio have more obvious influence on the dynamic responses of the blades compared to the tower. The dispersion of the displacement responses is larger in the operating condition compared to the parked condition. The maximum displacements of the tower and blades are larger in the operating condition than those in the parked condition.

Journal Pre-proof

(2) The yielding and buckling of the wind turbine tower is very unlikely to occur when the wind speeds are within the cut-in and cut-out range in either the operating or parked conditions. However, the probabilities of the limit state exceedance of the blades are more apparent in both conditions.

(3) The aerodynamic damping and the pitch control system have a considerable influence on the wind-induced displacement responses of the wind turbine, which slow down the increasing rate of the displacement responses with the increasing of the wind speed.

It should be noted that the fragility of the wind turbine in the in-plane direction is not developed in the present study due to the lack of an appropriate damage criterion of the in-plane responses for the blades as discussed in the paper, which needs to be further investigated in the future. Moreover, soil-structure interaction which might influence the structural responses is not considered in the present study either, and future studies on this interesting topic are suggested.

Acknowledgements

The authors would like to acknowledge the support from Australian Research Council Discovery Project DP190103279 for carrying out this research. The first author gratefully acknowledges the financial support from Curtin International Postgraduate Research Scholarship (CIPRS).

References

[1] Global Wind Energy Council (GWEC), https://gwec.net/51-3-gw-of-global-wind-capacity-installed-in-2018/.
[2] E.I. Katsanos, S. Thöns, C.T. Georgakis, Wind turbines and seismic hazard: a state-of-the-art review, Wind Energy 19 (11) (2016) 2113-2133.
[3] M.A. Asareh, W. Schonberg, J. Volz, Effects of seismic and aerodynamic load interaction on structural dynamic response of multi-megawatt utility scale horizontal axis wind turbines, Renew. Energy 86 (2016) 49-58.
[4] H. Zuo, K. Bi, H. Hao, Dynamic analyses of operating offshore wind turbines including soil-structure interaction, Eng. Struct. 157 (2018) 42-62.
[5] J. Chen, Y. Song, Y. Peng, S.R. Nielsen, Z. Zhang, An efficient rotational sampling method of wind fields for wind turbine blade fatigue analysis, Renew. Energy 146 (2019) 2170-2187.
[6] H. Zuo, K. Bi, H. Hao, C. Li, Influence of earthquake ground motion modelling on the dynamic responses of offshore wind turbines, Soil Dyn. Earthq. Eng. 121 (2019) 151-167.
[7] S.H. Ju, F.C. Su, Y.P. Ke, M.H. Xie, Fatigue design of offshore wind turbine jacket-type structures using a parallel scheme, Renew. Energy 136 (2019) 69-78.
[8] H. Wang, S. Ke, T. Wang, S. Zhu, Typhoon-induced vibration response and the working mechanism of large wind turbine considering multi-stage effects, Renew. Energy 153 (2020) 740-758.
[9] J. Zhu, Z. Zhou, X. Cai, Multi-objective aerodynamic and structural integrated optimization design of wind turbines at the system level through a coupled blade-tower model, Renew. Energy 150 (2020) 523-537.
[10] P.J. Murtagh, A. Ghosh, B. Basu, B.M. Broderick, Passive control of wind turbine vibrations including blade/tower interaction and rotationally sampled turbulence, Wind Energy 11(4) (2008) 305-317.
[11] S. Colwell, B. Basu, Tuned liquid column dampers in offshore wind turbines for structural control, Eng. Struct. 31(2) (2009) 358-368.
[12] H. Zuo, K. Bi, H. Hao, Using multiple tuned mass dampers to control offshore wind turbine vibrations under multiple hazards, Eng. Struct. 141 (2017) 303-315.
[13] J. Chen, Y. Zhao, O. Cong, M. He, Vibration control using double□response damper and site measurements on wind turbine, Struct. Control Health Monit. (2018) e2200.

Journal Pre-proof

[14] T. Buckley, P. Watson, P. Cahill, V. Jaksic, V. Pakrashi, Mitigating the structural vibrations of wind turbines using tuned liquid column damper considering soil-structure interaction, Renew. Energy 120 (2018) 322-341.
[15] H. Zuo, K. Bi, H. Hao, Mitigation of tower and out-of-plane blade vibrations of offshore monopile wind turbines by using multiple tuned mass dampers, Struct. Infrastruct. Eng. 15 (2019) 269-284.
[16] H. Zuo, K. Bi, H. Hao, A state-of-the-art review on the vibration mitigation of wind turbines, Renew. Sust. Energy Rev. 121 (2020) 109710.
[17] I. Prowell, M. Veletzos, A. Elgamal, J. Restrepo, Experimental and numerical seismic response of a 65 kw wind turbine, J. Earthq. Eng. 13 (2009) 1172-1190.
[18] R.A. Kjørlaug, A.M. Kaynia, Vertical earthquake response of megawatt-sized wind turbine with soil-structure interaction effects, Earthq. Eng. Struct. Dyn. 44 (2015) 2341-2358.
[19] P.J. Murtagh, B. Basu, B.M. Broderick, Along-wind response of a wind turbine tower with blade coupling subjected to rotationally sampled wind loading, Eng. Struct. 27 (2005) 1209-1219.
[20] M. Hansen, Aerodynamics of wind turbines 2nd edition, Earthscan, London, 2008.
[21] M. Harte, B. Basu, S.R.K. Nielsen, Dynamic analysis of wind turbines including soil-structure interaction, Eng. Struct. 45 (2012) 509-518.
[22] B. Fitzgerald, B. Basu, S.R.K. Nielsen, Active tuned mass dampers for control of in-plane vibrations of wind turbine blades, Struct. Control Health Monit. 20 (2013) 1377-1396.
[23] M.A. Lackner, M.A. Rotea, Passive structural control of offshore wind turbines, Wind Energy 14 (2011) 373-388.
[24] G.M. Stewart, M.A. Lackner, The impact of passive tuned mass dampers and wind-wave misalignment on offshore wind turbine loads, Eng. Struct. 73 (2014) 54-61.
[25] J.M. Jonkman, M.L. Buhl Jr, FAST user's guide-updated, Colorado, USA, National Renewable Energy Laboratory (NREL), 2005.
[26] L. Dueñas-Osorio, B. Basu, Unavailability of wind turbines due to wind-induced accelerations, Eng. Struct. 30 (2008) 885-893.
[27] A. Quilligan, A. O'Connor, V. Pakrashi, Fragility analysis of steel and concrete wind turbine towers, Eng. Struct. 36 (2012) 270-282.
[28] M. Mardfekri, P. Gardoni, Probabilistic demand models and fragility estimates for offshore wind turbine support structures, Eng. Struct. 52 (2013) 478-487.
[29] D.H. Kim, S.G. Lee, I.K. Lee, Seismic fragility analysis of 5 MW offshore wind turbine, Renew. Energy 65 (2014) 250-256.
[30] A. Patil, S. Jung, O. S. Kwon, Structural performance of a parked wind turbine tower subjected to strong ground motions, Eng. Struct. 120 (2016) 92-102.
[31] M.A. Asareh, W. Schonberg, J. Volz, Fragility analysis of a 5-MW NREL wind turbine considering aero-elastic and seismic interaction using finite element method, Finite Elem. Anal. Des. 120 (2016) 57-67.
[32] C. Yuan, J. Chen, J. Li, Q. Xu, Fragility analysis of large-scale wind turbines under the combination of seismic and aerodynamic loads, Renew. Energy 113 (2017) 1122-1134.
[33] S.T. Hallowell, A.T. Myers, S.R. Arwade, W. Pang, P. Rawal, E.M. Hines, J.F. Hajjar, C. Qiao, V. Valamanesh, K. Wei, Hurricane risk assessment of offshore wind turbines, Renew. Energy 125 (2018) 234-249.
[34] A.F. Mensah, L. Dueñas-Osorio, Improved reliability of wind turbine towers with tuned liquid column dampers (TLCDs), Struct. Saf. 47 (2014) 78-86.
[35] B. Fitzgerald, S. Sarkar, A. Staino, Improved reliability of wind turbine towers with active tuned mass dampers (ATMDs), J. Sound Vib. 419 (2018) 103-122.
[36] J. Jonkman, S. Butterfield, W. Musial, G. Scott, Definition of a 5-MW reference wind turbine for offshore system development Technical Report No. NREL/TP-500-38060, Colorado, USA, National Renewable Energy Laboratory (NREL), 2009.
[37] T. Burton, N. Jenkins, D. Sharpe, E. Bossanyi, Wind energy handbook 2nd edition, John Wiley & Sons, 2011.
[38] K. Bi, H. Hao, Using pipe-in-pipe systems for subsea pipeline vibration control, Eng. Struct. 109 (2016) 75-84.
[39] DNV, DNV-RP-C205: Environmental conditions and environmental loads, Norway: Det Norske Veritas (2010).
[40] S. Bisoi, S. Haldar, Dynamic analysis of offshore wind turbine in clay considering soil-monopile-tower interaction, Soil Dyn. Earthq. Eng. 63 (2014) 19-35.
[41] L. Arany, S. Bhattacharya, J.H. Macdonald, S.J. Hogan, Closed form solution of eigen frequency of monopile supported offshore wind turbines in deeper waters incorporating stiffness of substructure and SSI, Soil Dyn. Earthq. Eng. 83 (2016) 18-32.

Journal Pre-proof

626 [42] K. Hasselmann, T. Barnett, E. Bouws, H. Carlson, D. Cartwright, K. Enke, J. Ewing, H. Gienapp, D.
627 Hasselmann, P. Kruseman, Measurements of wind-wave growth and swell decay during the Joint North Sea
628 Wave Project (JONSWAP), Deutches Hydrographisches Institut, 1973.
629 [43] J. Zhang, Y. Huo, Evaluating effectiveness and optimum design of isolation devices for highway bridges
630 using the fragility function method, Eng. Struct. 31 (2009) 1648-1660.
631 [44] C. Li, H. Hao, H. Li, K. Bi, Seismic fragility analysis of reinforced concrete bridges with chloride induced
632 corrosion subjected to spatially varying ground motions, Int. J. Struct. Stab. Dyn. 16 (2016) 1550010.
633 [45] C. Li, H. Li, H. Hao, K. Bi, B. Chen, Seismic fragility analyses of sea-crossing cable-stayed bridges
634 subjected to multi-support ground motions on offshore sites, Eng. Struct. 165 (2018) 441-456.
635 [46] DNV, DNV-OS-J101: Design of offshore wind turbine structures, Copenhagen, Denmark, 2014.
636 [47] C.A. Dimopoulos, C.J. Gantes, Experimental investigation of buckling of wind turbine tower cylindrical
637 shells with opening and stiffening under bending, Thin-Walled Struct. 54 (2012) 140-155.
638 [48] L. Guo, S. Yang, H. Jiao, Behavior of thin-walled circular hollow section tubes subjected to bending, Thin-
639 Walled Struct. 73 (2013) 281-289.
640 [49] DNV, Risø National Laboratory, Guidelines for design of wind turbines 2nd edition, Denmark, 2002.

Journal Pre-proof

Journal Pre-proof

Highlights:

(1) Detailed three-dimensional FE model of wind turbine is developed;

(2) Influences of uncertainties in material and damping on structural responses are studied;

(3) Fragilities of both the tower and blades are investigated;

(4) Fragility of wind turbine under different operational conditions is examined.

Journal Pre-proof

Journal Pre-proof

Declaration of interests

☒ The authors declare that they have no known competing financial interests or personal relationships that could have appeared to influence the work reported in this paper.

☐The authors declare the following financial interests/personal relationships which may be considered as potential competing interests:

Journal Pre-proof